Numerical characterization of the aerodynamics in fixed-grate biomass burners

Adeline Rezeau*, Juan A. Ramírez, Luis I. Díez, Javier Royo

CIRCE – Center of Research of Energy Resources and Consumptions
Department of Mechanical Engineering, University of Zaragoza
María de Luna 3, 50018 Zaragoza, Spain

Abstract

This paper investigates the numerical simulation of the aerodynamics of biomass burners operating in small-scale, fixed-grate technologies. The efficiency of these boilers is largely determined by the fluid patterns originated in the combustion chamber, as a consequence of the interaction of primary and secondary inlets. A set of CFD computations have been carried out for a case-study burner, seeking the comparison for the isothermal-flow solutions given by Reynolds Averaged Navier-Stokes equations (RANS) and by Unsteady RANS equations (URANS). The influence of both spatial and temporal discretization is discussed, using the Grid Convergence Index (GCI) based on Richardson extrapolation. The results indicate that RANS solutions are slightly more sensible to grid parameters, while URANS solutions show a better convergence behavior. Validation has been reasonably achieved by comparing the URANS velocity profiles against experimental measurements. As a consequence, a mathematical tool is now available to support design modifications of the biomass burner, combining simplicity, reliability and economy.

Keywords

Grate burners; CFD; URANS; Grid Convergence Index (GCI)

---

* Corresponding autor. Tel.: +34 976 762 582. Fax: +34 976 732 078. E-mail: arezeau@unizar.es

Nomenclature

D_H	hydraulic diameter	m
e	relative error, as defined by Eq. (5)	–
GCI	grid convergence index, as defined by Eq. (4)	–
h_i	averaged cell size of the i^{th} grid, as defined by Eq. (3)	m
k	turbulent kinetic energy	m^2/s^2
L	characteristic length	m
N_i	number of cells of the i^{th} grid	–
p	static pressure; order of accuracy	Pa; –
r	refinement factor	–
t	time	s
U_D	experimental data uncertainty	–
U_{SMA}	simulation uncertainty due to modeling assumptions	–
U_{SN}	simulation uncertainty due to numerical resolution	–
U_{SPD}	simulation uncertainty due to prescribed input data	–
V	volume	m^3
v	velocity	m/s
v´	velocity fluctuation	m/s
x	x-coordinate, x-component	–
y	y-coordinate, y-component	–
z	z-coordinate, z-component	–

Greek symbols

ε	turbulent dissipation rate	m^2/s^3
μ	fluid viscosity	Pa.s
ρ	fluid density	kg/m^3
σ	standard deviation error, as defined by Eq. (7)	–

Subscripts

1 coarse grid

2 medium grid

3 fine grid

max maximum value

min minimum value

1. Introduction

Packed bed technologies for solid biofuels combustion are increasingly used, mainly because of their simple operation, wide fuel flexibility and low operational costs [1-3]. Application of grate burners currently ranges from small-scale units for domestic heat supply to large-scale utility boilers for power generation, thus emerging different firing technologies like fixed, moving, vibrating or traveling grates [4-6]. Even though remarkable improvements have been accomplished in the design of modern grate boilers for biomass combustion, recording growing figures for carbon burnout and heat transfer rates, additional work is still to be done in small-size burners to increase combustion efficiency, reduce pollutants and improve operation and control.

In grate burners, the location and distribution of primary and secondary air inlets drastically affects the combustion efficiency [6-11], since fluid-dynamics can be significantly altered by minor modifications of the air flow distribution. Although this is a well known fact, scarce attention has been typically paid by manufacturers in optimizing the air distributions of small-scale units, since their developments have been usually based on experience and empirical results. In the Spanish context, a certain explanation is the necessity of cutting costs to gain in competitiveness against gas-fired boilers, which require lower investments but provide higher thermal efficiencies. Under these circumstances, the demand of expensive experimental rigs and advanced instrumentation has ruled out the testing of new prototypes under well-controlled combustion conditions. However a balance can be even attained between the necessity of improving the performance

and the constraint of maintaining the cost: cold-flow testing can be easily carried out, without special requirements for operating conditions and instrumentation, providing results to computer-assisted tools developed to improve the aerodynamics of grate burners. Although the actual flow is obviously different when combustion occurs, the general structure of primary-secondary air interactions can be adequately characterized under isothermal conditions.

Summing up, the frame of this investigation is to develop a CFD-based model to predict the thermal performance of biomass-fired grate burners. This paper is focused in the first stage of the research, aiming at the aerodynamic characterization of the furnace. The scope is twofold: firstly, to check the convenience of solving URANS equations to simulate the complex fluid flow structure, and secondly, to discuss the optimum pairs of grid size and time step to be used in the validation and future computations. This will also be useful for a further coupling of mathematical models accounting for combustion, heat transfer and solid-gas interaction.

The results from CFD computations are going to be validated against experimental data gathered during tests. As suggested by Coleman et al. [12-13], see Fig. 1, different uncertainties arise when a numerical model is built up to reproduce a complex physical phenomenon, both in the simulation and the validation. As for the simulation process, three global uncertainties contribute to the total simulation error: U_{SMA}, U_{SPD} and U_{SN}. The modeling uncertainty, U_{SMA}, takes into account the deviations introduced by the model itself; e.g., the turbulence model used to simulate the correlations of velocity fluctuations in a turbulent flow, aside from other assumptions as incompressibility, two-dimensionality, etc. The uncertainty due to prescribed data, U_{SPD}, is related to the errors in inputs used to close the definition of the problem, as domain geometry or boundary conditions. Finally, the numerical uncertainty U_{SN} accounts for the deviations due to the numerical resolution of the governing equations. Coleman et al. underline the relevance of minimizing the effect of the latter, since it is usually related to the solution method and the discretization scheme, along with the type and size of the meshing or the unsteady consideration. Finally, the validation uncertainty is also affected by the experimental uncertainty U_D, viz. errors during the measurement and acquisition of process data.

CFD computation of a solid-fired boiler, which is an intricate reactive, multiphase, turbulent and radiative media, brings along dominant modeling uncertainties, due to the complexity of the underlying physical phenomena. This is eventually assumed, recognizing that only global trends may be expected. Nevertheless, computation of non-reactive, turbulent flows could be equally affected by modeling uncertainties or numerical uncertainties. Many turbulence models are currently available in commercial software and, in addition, there also exist many ways to grid a computational domain [14-15]. A lot of research activities are in-development in these fields and the results obtained by different works may sometimes be revealing. On one hand, some authors have found out that the grid refinement is more essential for results than the turbulence model used [14]. Yin et al. [16-17] added that the grid affects largely the CFD results, but they also indicated that the grid-independence cannot be really achieved even on a very fine mesh (when applied to large boilers). On the other hand, as for the turbulence modeling, several papers pinpoint the importance of temporal-averaging computations when calculating statistically unsteady flows [18-25]. The conclusion is that even if an accurate spatial discretization is applied, turbulent flows which are in fact time-dependent will fail to converge using a steady-state method. Very often, convergence problems with a steady simulation can be interpreted as a hint that the turbulent flow is unsteady and a time-stepping scheme would be appropriate.

In the present work, we compare the air velocity profiles in the case-study biomass grate burner obtained by RANS and URANS simulations. A grid refinement methodology is described and the spatial discretization errors are determined for the transient calculations by means of the Grid Convergence Index (GCI), based on Richardson extrapolation [26-28]. The temporal discretization errors are also identified, once the grid size is selected. Finally, the numerical results are validated against experimental data.

2. Description of the case-study

The case-study grate boiler is a 250 kW fuel input unit, designed to fire refined solid biofuels, usually called *pellets*. The burner is connected to a fume-tube boiler that supplies hot water at 90 ºC and atmospheric pressure. The fuel is introduced

by a screw feeder on a fixed, inclined stair-like grate; the movement of the bed is achieved by means of the fresh fuel pushing the particles already on the inclined grate. After the grate, but before the solids fall into the ash-pit hopper, a horizontal plate is included to increase residence time and achieve a better char burnout. Moreover, a pusher is activated at a specific frequency in order to move forward the bed material. An independent supply of primary and secondary air flow rates is provided each by its own fan. The updraft primary air is introduced by the horizontal bottom while additional primary air is also injected through the stair levels. The secondary jets are distributed by seventeen nozzles concentrically located along the walls, to burn the volatiles released from the bed. At nominal conditions, the air split is 240 Nm^3/h primary and 400 Nm^3/h secondary.

Figure 2 depicts the geometrical domain selected for CFD computations. The domain comprises the fuel inlet, the grate, the air ports, the combustion zone and the exit duct. The total size of the domain is 1.200 m long, 0.345 m wide and 0.502 m high.

3. CFD modeling and computation strategies

Calculation of the turbulent fluid flow within the computational domain requires the resolution of the momentum conservation equations, which under assumptions of incompressible flow and constant-properties are given by:

$$\rho\frac{\partial v}{\partial t}+\rho v\nabla\cdot v=-\nabla p+\mu\nabla\left(\nabla\cdot v\right)-\rho\nabla\left(v'v'\right)+\rho g \tag{1}$$

This expression is in fact the time-averaged of the so-called Reynolds Averaged Navier-Stokes equations, where turbulence is introduced by fast-frequency fluctuations around a mean value. The averages of the turbulent variables along the time are equal to their statistical means, i.e. the average of the fluctuations yields a nil value. This is a usual treatment for CFD simulation of turbulent flows in complex and/or large geometries, since direct numerical simulation of the turbulent variables would demand an extraordinary computational effort due to the extremely fine geometrical mesh and a time discretization. Correlation of velocity fluctuations arising in Eq. (1) has been modeled by the Realizable k-ε turbulence model [29], solving the conservation equations for two additional variables: the turbulent kinetic energy, k, and the turbulent dissipation rate, ε.

This method is widely used in industrial CFD computations, despite its limitations for irregular flow structures, since it offers a reasonable balance between computing requirements and engineering accuracy.

We have proceeded with steady-state (RANS) and unsteady (URANS) simulations in order to check the influence of temporal term consideration on the predictions. As Durbin [18] underlines, steady-state consideration — i.e., first term in Eq. (1) is not taken into account— lead to biased results when computing complex turbulent flows, due to the omission of the spikes (at vortex shedding frequencies) from the mean flow.

The boundary conditions prescribed at input sections –constant mass flow rates and temperatures– have been inferred from nominal operating data of the burner; we have assumed a proportional split of flow rates through injection nozzles as a function of their surface areas. The turbulence intensity has been set as 5%. Non-slip condition is considered for solid walls, with conventional law-of-the-wall profiles for turbulent boundary layer. A cero gauge pressure condition is assumed at the outlet section.

The calculations have been completed with the commercial software Fluent 6.3, using a pressure-based solver with an implicit formulation. The pressure-velocity coupling is calculated by the SIMPLE algorithm. The convergence stop criteria for all terms have been fixed at 10^{-4}.

We started prescribing a hybrid mesh of N_1 = 626 825 cells, made up of 65.5% hexahedral elements and 34.5% pyramidal elements. This will be called from now onwards the "coarse" grid. The pyramidal elements are selected to capture the geometric characteristics of the circular air nozzles. The size of the elements is variable to better reproduce the contour of the stair-like grate, smoothing the variations of the mesh from the central section of the boiler and avoiding skew angles (no elements having an equisize or equiangle skew above 0.96).

Two additional grids have been tested in order to ascertain the spatial discretization error of the computations, which represent a relevant contribution to the numerical uncertainty. This grid independence analysis aims to provide a prediction only depending on the modeling assumptions, but not on the mesh type or size. The so-called "medium" and "fine" grids are respectively made up of N_2 = 1 377 729 and N_3 = 3 249 952 elements (see Fig. 3). The summary of the grids characteristics is shown in Table 1. The maximum grid sizes have been selected

according to the recommended refinement factors r for the Grid Convergence Index (GCI) calculations, hereinafter discussed,

$$r = \frac{h_i}{h_{i+1}} = \left(\frac{N_{i+1}}{N_i} \right)^{1/3} \tag{2}$$

where the averaged cell size h of the i-th grid is given by:

$$h_i^3 = \frac{V}{N_i} \tag{3}$$

The computation methodology has been the following. Firstly, a converged solution for the steady-state fluid flow has been achieved, for each grid. These solutions are then used as initial condition for the unsteady calculations, initially using a time step of Δt = 0.10 s for a total interval of t = 1 000 s. This methodology enables to accelerate the convergence of the URANS to a statistically stationary solution. The influence of the time discretization is also analyzed by comparing the results for Δt = 0.10 s and Δt = 0.50 s. Finally, and once the discretization errors are minimized, the CFD predictions for velocities have been validated against experimental measurements in the burner.

4. Results and discussion

To introduce the analysis of the CFD predictions, velocity profiles are provided in the vertical mid y-z plane of the domain, at x = 0.172 m, according to the predominant flow direction. In this plane, four check-lines are chosen to depict the simulation results. The respective location of these lines is the following (see also Fig. 2): line A, y = 0.101 m; line B, y = 0.161 m; line C, y = 0.251 m; line D, y = 0.327 m.

Figure 4 displays the velocity profiles along these lines, obtained for the three tested meshes, both for RANS and URANS computations. In all cases, the influence of the air entries can be clearly seen; e.g. at lines A, B and C the high velocities correspond to the primary air entries through stair-liked grate (z < 0.3 m) and at lines C and D the velocity increase is due to the plenum and secondary air jets (z = 0.756 m). Also, it can be observed that the primary air injected through the horizontal plate barely influences, just the nearby flow.

Transient calculations for the three grids yield more similar results between each other than in the steady case, showing the latter a slightly greater dependence on the grid size, which is good agreement with similar previous experiences [16-17]. Nevertheless, the differences are very low. It can be also observed that velocities present a non-monotonic convergence for a number of points in the selected check-lines.

To confirm these statements and evaluate the spatial discretization errors still remaining in the transient calculations, we have adopted the Grid Convergence Index analysis, based on Richardson extrapolation [26-28]. For monotonic convergence points, this index is defined as

$$GCI_{21} = 1.5\frac{e_{21}}{r^p - 1} \tag{4a}$$

$$GCI_{32} = 1.5\frac{e_{32}}{r^p - 1} \tag{4b}$$

where r is the refinement factor given by Eq. (2), p is the order of accuracy and e is the relative error given by:

$$e_{21} = \left|\frac{v_1 - v_2}{v_1}\right| \tag{5a}$$

$$e_{32} = \left|\frac{v_2 - v_3}{v_2}\right| \tag{5b}$$

It is worth noting that GCI analysis does not provide an adequate estimate of spatial discretization errors for those nodes showing non-monotonic convergence, since GCI reaches high values but not indicating unsatisfactory results [26]. This is the case of several check-points in our computations, where the velocity values for the three grids, at a same node, agree with the condition given by Eq. (6):

$$\frac{v_3 - v_2}{v_2 - v_1} < 0 \tag{6}$$

To streamline the analysis for these nodes, the spatial discretization error can be assessed by a standard deviation error calculated as

$$\sigma_2 = \frac{1}{2}\left(\frac{v_{\max} - v_{\min}}{v_2}\right) \tag{7}$$

where v_{max} and v_{min} are given by

$$v_{\max} = \max(v_1, v_2, v_3) \tag{8a}$$

$$v_{\min} = \min(v_1, v_2, v_3) \tag{8b}$$

The velocities comparison has to be done at exactly the same domain positions for the three meshes, thus interpolations of the "coarse" and the "medium" predictions are required to face them against the values computed when the "fine" grid is used. Table 2 summarizes the mean values of GCI and σ_2 in the lines A to D. Mean values for GCI_{32} index ranges from 4.7% to 13.8%. Figure 5 translates the minimum and maximum values of GCI_{21}, GCI_{32} and σ_2 into the velocity profiles at lines A to D, by means of deviation bars. The comparisons throughout the domain have pointed out that GCI_{32} values are lower than GCI_{21} values, which is in agreement with the expected results. Also, when we turn the focus in the relative error e, it is clear that mean values for e_{32} are also lower than e_{21}, now ranging from 2.9% to 9.6%. Therefore, reduction of the grid size has led to coherent trends of the spatial discretization errors.

The time step used for URANS computations shown in Fig. 4 and 5 was fixed in a value of Δt = 0.1 s. It should be noted that some guides are available in the literature to choose a time step based on characteristic length of the domain and the maximum velocity inside it, see elsewhere [30]; however these guides are focused in detecting an oscillatory or periodic behavior of the pressure or velocity fields, what is out of the reach of this work. We selected a value of 0.1 s, and, just for a criticism exercise, deliberately enlarged the time step by a factor of 5, from 0.1 s to 0.5 s. Comparative results between both unsteady simulations are displayed in Fig. 6 for the check-lines A to D. It can be observed that both time steps predicts a very similar value of velocity. Since time discretization is not a so critical parameter for isothermal simulations from the point of computing demands, we kept the minimum value from the beginning. However, if a complete non-isothermal simulation is intended, a further discussion of time step selection should be done to determine the optimum time step to achieve independent solutions with reasonable computing times.

Finally, validation of the CFD computations has been undertaken by comparing the predicted velocity figures against experimental values gathered during tests. A campaign of measurements was executed, at nominal load and isothermal

conditions. Velocities were taken inserting the probe through the three different ports. A mean velocity value was obtained for each of the sampling points, located at different lengths from the wall, to be compared with numerical computations.

Table 3 shows the URANS predictions against experimental velocities. Predicted values show a reasonable agreement, but differences are present at some locations. It seems to be that injection of primary air through the stair is preferential at $x < 0.25$ m. Observing the velocity results depicted in Fig. 7, it is predictable that the main recirculation zone in the burner would present an air defect during combustion of solid biofuels in the bed, especially above the stair-like grate. Location of secondary air injections does not compensate this effect, since they are located in an excessive back position of the burner section. The outcome is that aerodynamics of the burner could be improved aiming at more uniform air splits, by reallocating the fans and the air distribution nozzles.

5. Conclusions

A CFD-based tool has been developed and validated to characterize the aerodynamics of small-scale grate boilers. A rigorous step-by-step numerical analysis has been completed, based on Richardson extrapolation, then reducing the numerical uncertainty due to grid- and time-dependence of the results. URANS solutions have shown a slight better behavior as for obtaining an accurate solution, which is good agreement with previous experiences for similar simulations.

Validation has been reasonably achieved by comparing the URANS velocity profiles against experimental measurements in a case-study boiler. The results have also revealed some irregularities in air distributions that should be corrected according to CFD predictions. Application of this mathematical tool is already supporting aerodynamic modifications of the existing designs, without requiring stringent computing requirements or economic funds.

References

[1] Nussbaumer, T., Combustion and co-combustion of biomass: fundamentals, technologies and primary measures for emission reduction, Energy & Fuels **17** (2003) 1510-1521.

[2] Strehler, A., Technologies of wood combustion, Ecological Engineering **16** (2000) 25-40.

[3] Verma, V. K., Bram, S., De Ruyck, J., Small scale biomass heating systems: Standards, quality labeling and market driving factors − An EU outlook, Biomass and Bioenergy **33** (2009) 1393-1402.

[4] Yin, C., Rosendahl, L. A., Kær, S. K., Grate-firing of biomass for heat and power production, Progress in Energy and Combustion Science **34** (2009) 725-754.

[5] van den Broek, R., Faaij, A., van Wijk, A., Biomass combustion for power generation, Biomass and Bioenergy **11** (1996) 271-281.

[6] Van Loo, S., Koppejan, J., The Handbook of Biomass Combustion and Co-Firing, Earthscan, London, 2008.

[7] Kuo, J. T., Hsu, W. S., Yo, T. C., Effect of air distribution on solid fuel bed combustion, Journal of Energy Resources Technology **113** (1997) 120-128.

[8] Nasserzadeh, V., Swithenbank, J., Jones, B., Effect of high speed secondary air jets on the overall performance of a large MSW incinerator with a vertical shaft, Combustion Science and Technology **92** (1993) 389-422.

[9] Rönnbäck, M., Axell, M., Gustavsson, L., Thunman, H., Leckner, B., Combustion processes in a biomass fuel bed − Experimental results, in: Progress in Thermochemical Biomass Conversion, A. V. Bridgwater (Ed.), Blackwell Science Ltd, 2001.

[10] Staiger, B., Unterberger, S., Berger, R., Hein, K. R. G., Development of an air staging technology to reduce NO_x emissions in grate fired boilers, Energy **30** (2005) 1429-1438.

[11] Zhao, W., Li, Z., Wang, D., Zhu, Q., Sun, R., Meng, B., Zhao, G., Combustion characteristics of different parts of corn straw and NO formation in a fixed bed, Bioresource Technology **99** (2008) 2956-2963.

[12] Coleman, H. W., Stern, F., Uncertainties and CFD code validation, Journal of Fluids Engineering **119** (1997) 795 -803.

[13] Coleman, H. W., Some observations on uncertainties and the verification and validation of a simulation, Journal of Fluids Engineering **125** (2003) 733-735.

[14] Karvinen, A., Ahlstedt, H., Ala-Juusela, J., Hellsten, A., Huhtanen, R., Effects of grid density and turbulence models on a jet in crossflow, Seventh European Conference on Industrial Boilers and Furnaces, Porto, Portugal, 2006.

[15] Boudier, G., Staffelbach, G., Gicquel, L.Y.M., Poinsot, T. J., Mesh dependency of turbulent reacting large-eddy simulations in a gas turbine combustion chamber, in: Quality and Reliability of Large-Eddy Simulations, Ercoftac Series, Vol. 12, Springer Netherlands, 2008.

[16] Yin, C., Rosendahl, L. A., Kær, S. K. Numerical simulation of a biomass-fired grate boiler, Seventh European Conference on Industrial Boilers and Furnaces, Porto, Portugal, 2006.

[17] Yin, C., Rosendahl, L. A., Kær, S. K., Clausen, S., Hvid, S.L., Hille, T., Mathematical modeling and experimental study of biomass combustion in a thermal 108 MW grate-fired boiler, Energy & Fuels **22** (2008) 1380-1390.

[18] Durbin, P.A., A perspective on recent developments in RANS modeling, in: Engineering Turbulence Modeling and Experiments, W. Rodi and N. Fueyo (Eds), Elsevier Science, 2002.

[19] Fröhlich, J., von Terzi, D., Hybrid LES/RANS methods for the simulation of turbulent flows, Progress in Aerospace Sciences **44** (2008) 349-377.

[20] Tucker, P. G., Pan, Z., URANS computations for a complex internal isothermal flow, Computer Methods in Applied Mechanics and Engineering, 190 (2001) 2893-2907.

[21] Le, A., Hai, L. X., Sharifi, V. N., Swithenbank, J., System approach from biomass combustion in packed bed reactor, Asean Journal of Chemical Engineering **7** (2007) 16-29.

[22] Sadiki, A., Maltsev, A., Wegner, B., Flemming, F., Kempf, A., Janicka, J., Unsteady methods (URANS and LES) for simulation of combustion systems, International Journal of Thermal Sciences **45** (2006) 760-773.

[23] Iaccarino, G., Ooi, A., Durbin, P.A., Behnia, M., Reynolds averaged simulation of unsteady separated flow, International Journal of Heat and Fluid Flow **24** (2003) 147-156.

[24] Delibra, G., Borello, D., Hanjalic, K., Rispoli, F., URANS of flow and endwall heat transfer in a pinned passage relevant to gas-turbine blade cooling, International Journal of Heat and Fluid Flow **30** (2009) 549-560.

[25] Wegner, B., Maltsev, A., Schneider, C., Sadiki, A., Dreizler, A., Janicka, J., Assessment of unsteady RANS in predicting swirl flow instability based on LES and experiments, International Journal of Heat and Fluid Flow **25** (2004) 528-536.

[26] Celik, I., Zhang, W.-M., Calculation of numerical uncertainty using Richardson extrapolation: Application to some simple turbulent flow calculations, Journal of Fluids Engineering **117** (1995) 439-445.

[27] Celik, I., Ghia, U., Roache, P. J., Freitas, C. J., Coleman, H., Raad, P. E., Procedure for estimation and reporting of uncertainty due to discretization in CFD applications, Journal of Fluids Engineering **130** (2008) 078001.

[28] Stern, F., Wilson, R., Coleman, H. W., Paterson, E., Comprehensive approach to verification and validation of CFD simulations − Part 1: Methodology and procedures, Journal of Fluids Engineering **123** (2001) 793-802.

[29] Shih, T.-H., Liou, W. W., Shabbir, A., Yang, Z., Zhu, J., A new k-ε eddy viscosity model for high Reynolds number turbulent flows, Computers & Fluids **24** (1995) 227-238.

[30] Velilla, J., Estudio del flujo en el interior del conducto de extracción de sólidos de un ciclón de una central térmica de lecho fluido a presión (Analysis of the fluid flow in a cyclone of a pressurized fluidized bed boiler), Ph.D. Thesis, University of Zaragoza, 2004.

Figures caption

Figure 1. Uncertainties sources in numerical simulation and validation (adapted from [13]).

Figure 2. Geometrical domain for CFD computation and location of check-lines A to D.

Figure 3. Refined grids for assessment of numerical discretization error.

Figure 4. Comparison of velocity profiles given by RANS and URANS computations for the three grids, at check-lines A to D.

Figure 5. Distribution of spatial discretization errors in the medium grid, for URANS computations, at check-lines A to D.

Figure 6. Effect of time discretization in velocity predictions, for URANS computations, at check-lines A to D.

Figure 7. Velocity profiles for URANS solution, in the mid y-z plane, at x = 0.172 m, and in the secondary air jets section, at z = 0.756.

Tables caption

Table 1. Characteristics of the three grids used for the grid convergence test.

Table 2. Mean spatial discretization errors, for URANS computations with the three grids, at check-lines A to D.

Table 3. Comparison of URANS velocity predictions against experimental measurements, at three different ports.

Figure 1. Uncertainties sources in numerical simulation and validation (adapted from [13]).

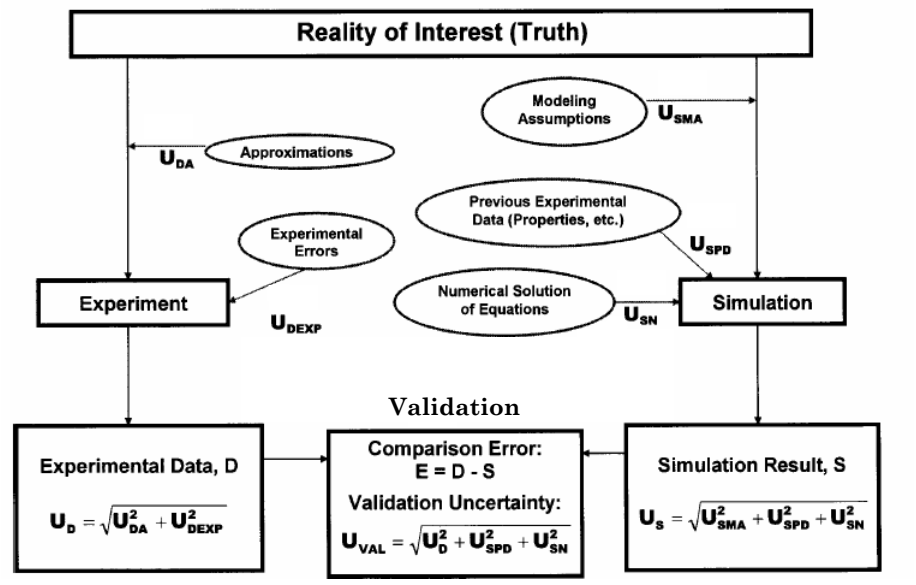

Figure 2. Geometrical domain for CFD computation and location of check-lines A to D.

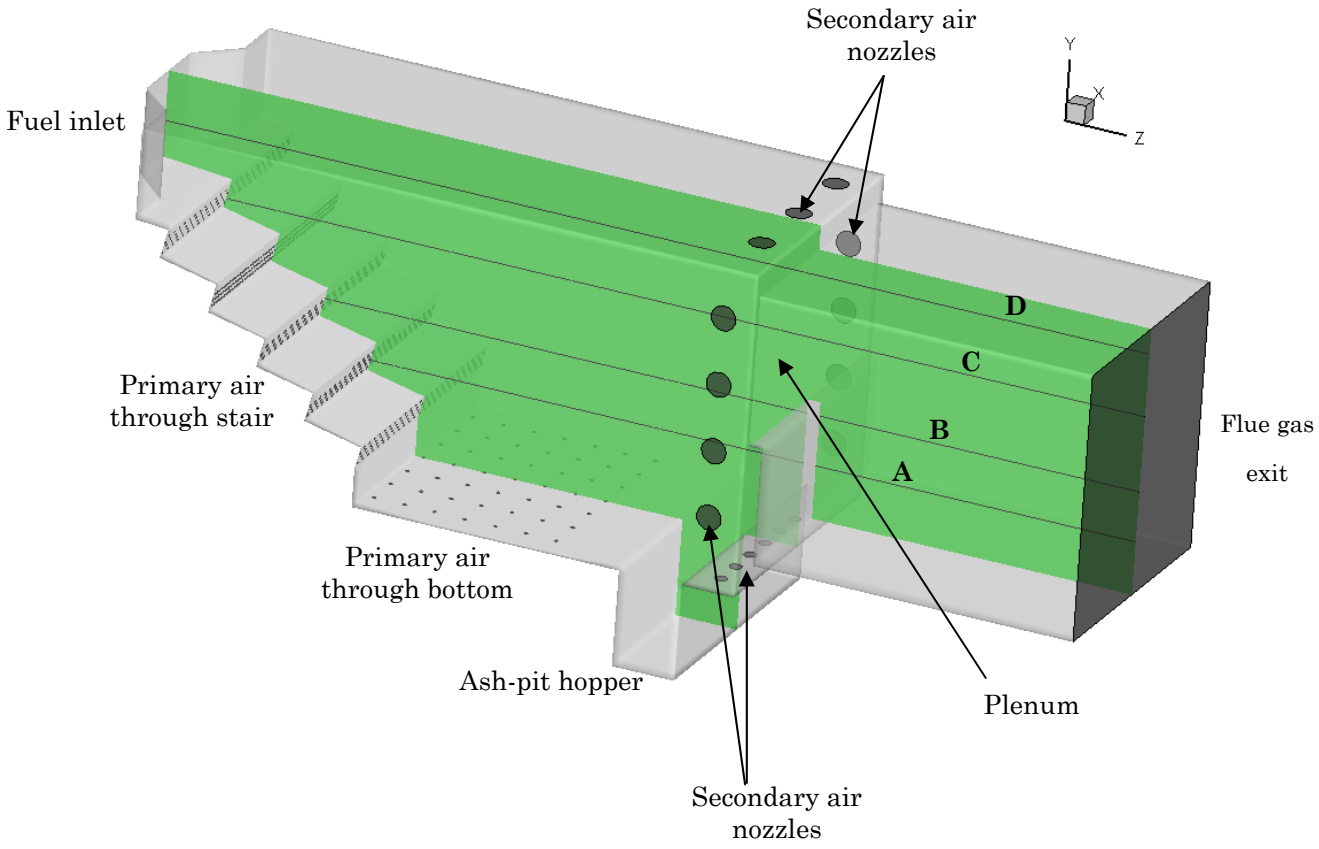

Figure 3. Refined grids for assessment of numerical discretization error.

Coarse

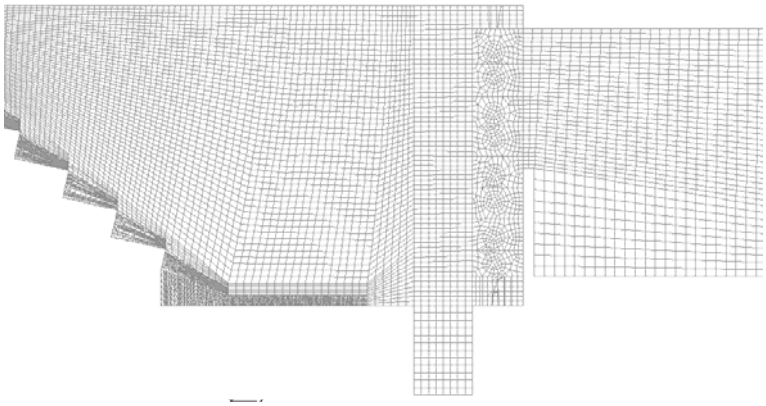

Medium

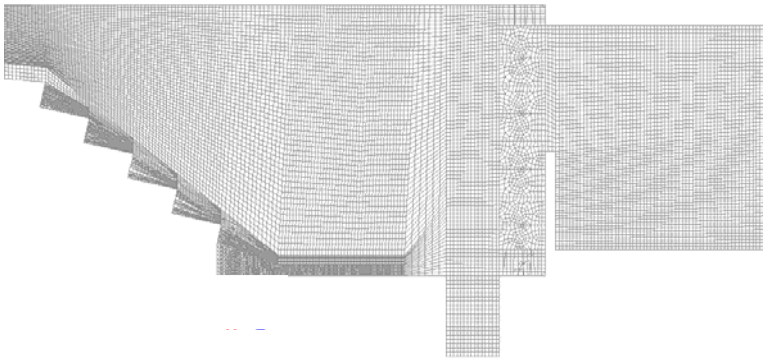

Fine

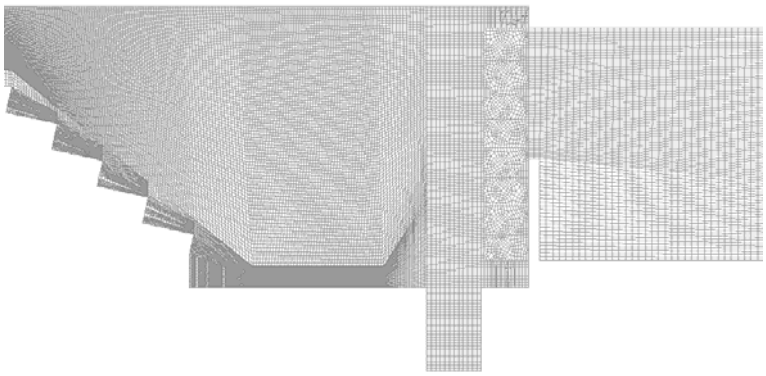

Figure 4. Comparison of velocity profiles given by RANS and URANS computations for the three grids, at check-lines A to D.

	RANS	URANS
A	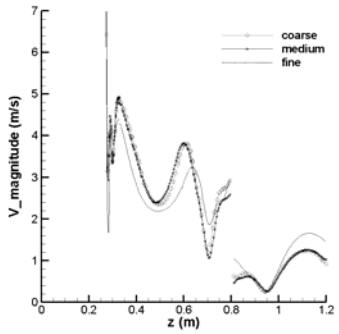	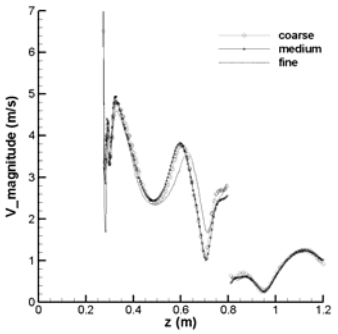
B	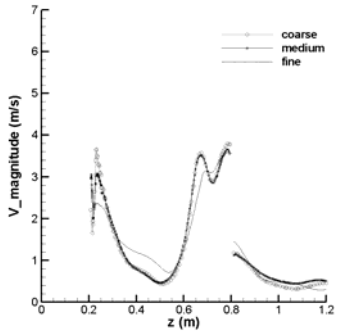	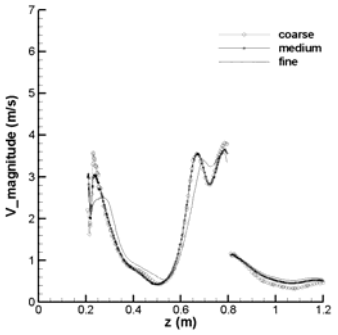
C	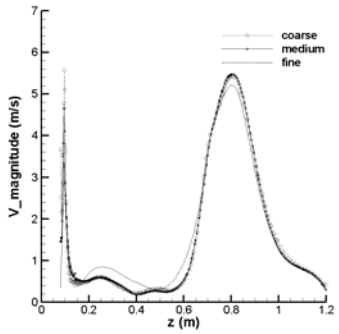	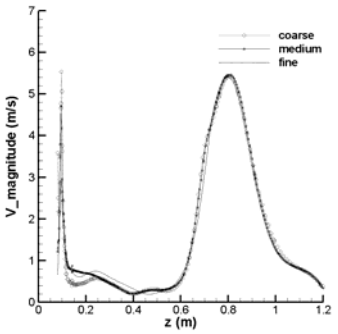
D	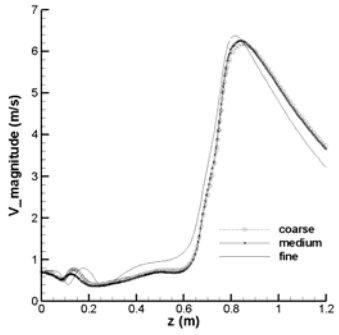	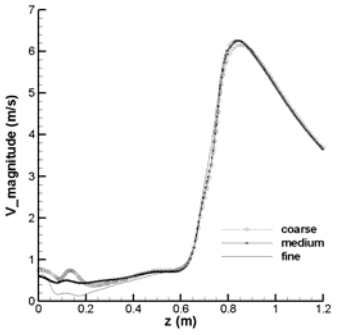

Figure 5. Distribution of spatial discretization errors in the medium grid, for URANS computations, at check-lines A to D.

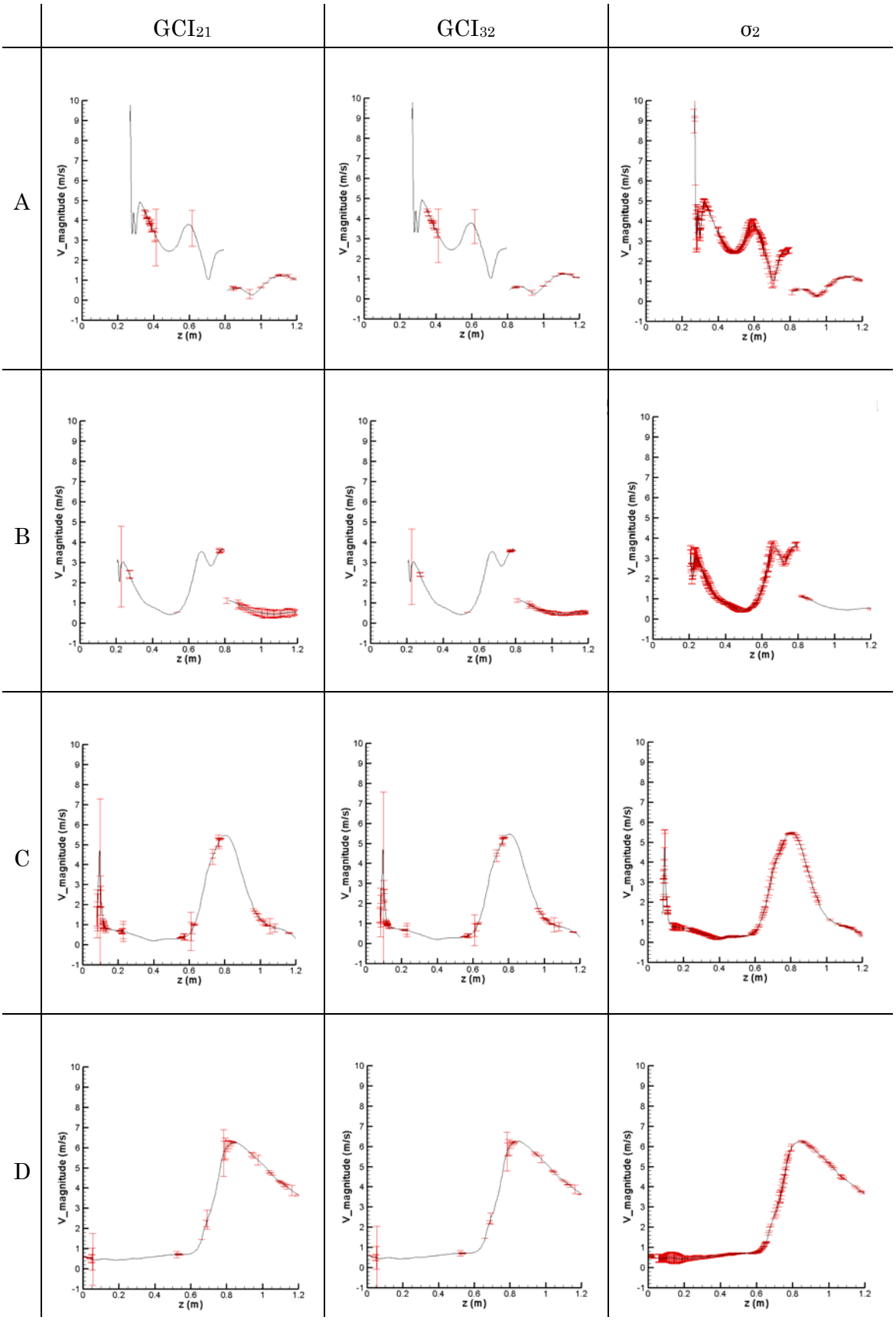

Figure 6. Effect of time discretization in velocity predictions, for URANS computations, at check-lines A to D.

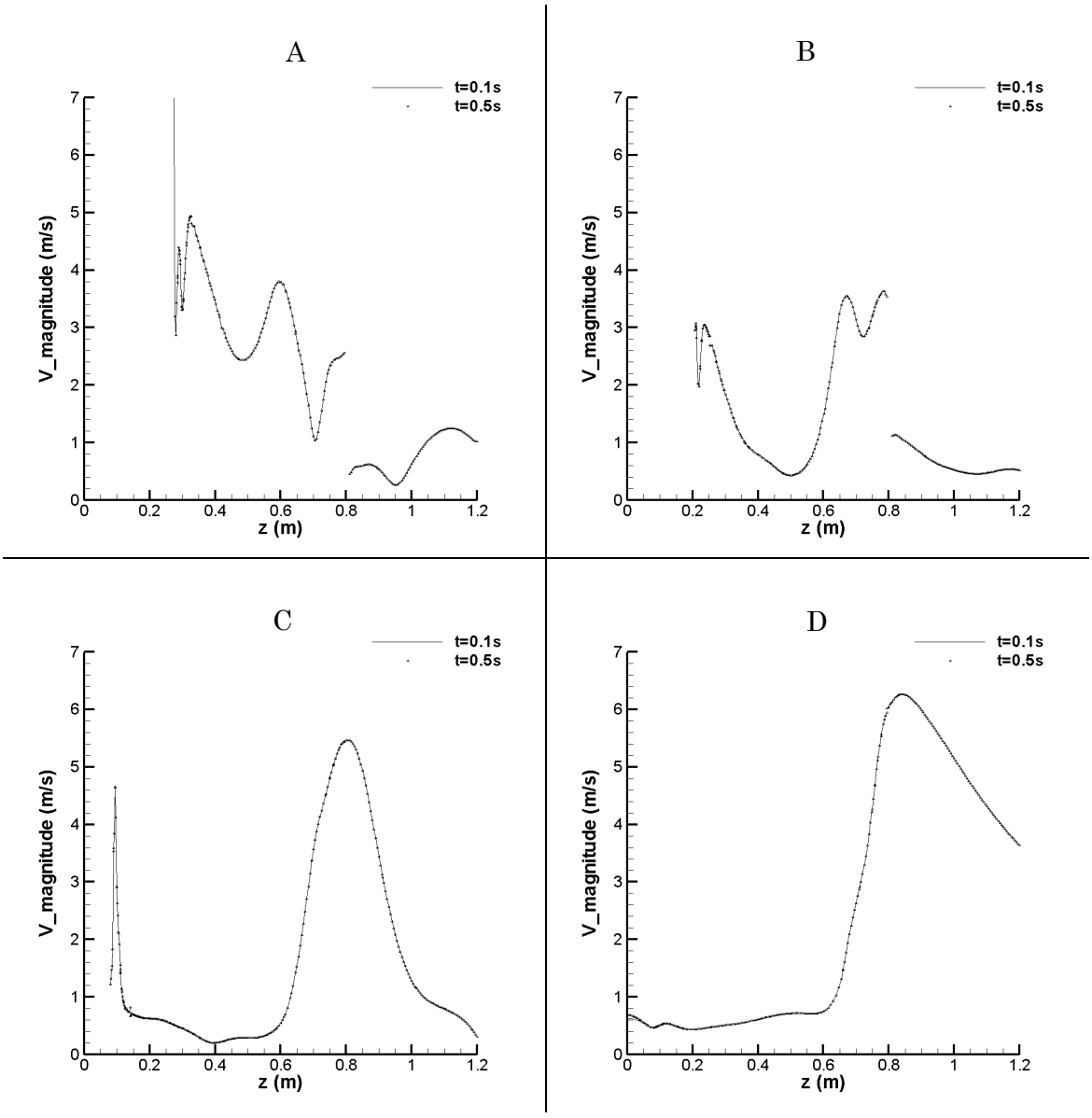

Figure 7. Velocity profiles for URANS solution, in the mid y-z plane, at x = 0.172 m, and in the secondary air jets section, at z = 0.756.

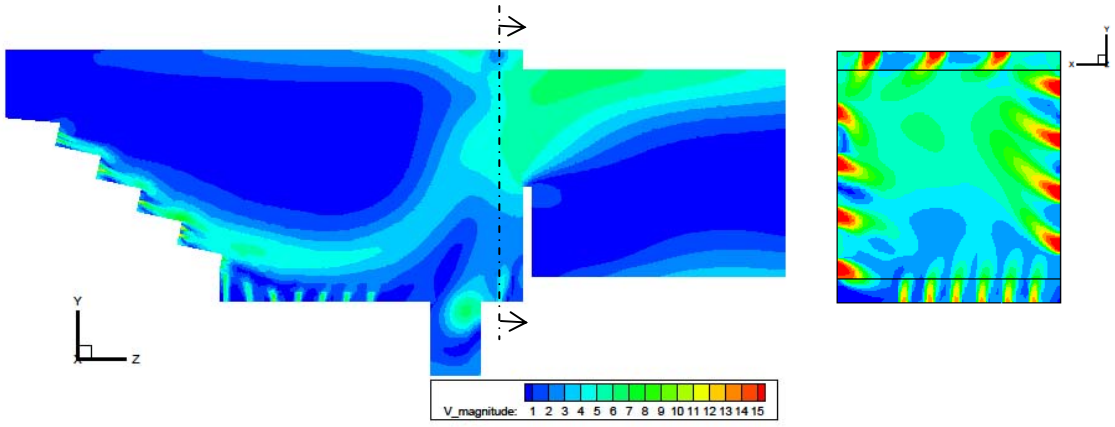

Table 1. Characteristics of the three grids used for the grid convergence test.

Grid name	Coarse	Medium	Fine
Number of cells, N	626 825	1 377 729	3 249 952
Averaged cell size, h (m)	5.88×10^{-3}	4.53×10^{-3}	3.40×10^{-3}
Refinement factor, r	–	1.300	1.331

Table 2. Mean spatial discretization errors, for URANS computations with the three grids, at check-lines A to D.

	Line A	Line B	Line C	Line D
Fraction of points showing monotonic convergence (%)	12.9	19.0	23.1	13.7
Grid convergence index, GCI_{21} (%)	7.9	27.6	19.3	14.4
Grid convergence index, GCI_{32} (%)	4.7	11.9	11.8	13.8
Standard deviation error, σ_2 (%)	7.0	10.9	13.2	18.4
Relative error, e_{21} (%)	7.2	21.6	24.2	7.5
Relative error, e_{32} (%)	2.9	9.6	8.2	4.1

Table 3. Comparison of URANS velocity predictions against experimental measurements, at three different ports.

	Experimental (m/s)	URANS (m/s)
Port #1 (y = 0.347 m, z = 0.615 m)		
x = 0.05 m	1.41 ± 0.17	1.04
x = 0.15 m	1.57 ± 0.14	1.21
Port #2 (y = 0.194 m, z = 0.615 m)		
x = 0.25 m	1.36 ± 0.18	1.63
x = 0.35 m	1.56 ± 0.14	1.82
Port #3 (x = 0.172 m, z = 0.367 m)		
y = 0.20 m	0.52 ± 0.08	0.56
y = 0.30 m	1.18 ± 0.16	1.78